Enhanced Long-Path Electrical Conduction in ZnO Nanowire Array Devices Grown via Defect-Driven Nucleation

Alex M. Lord,*,[†,#] Michael B. Ward,[‡,#] Jonathan E. Evans,[†] Philip R. Davies,[§] Nathan A. Smith,[∥] Thierry G. Maffeis,[⊥] and Steve P. Wilks[∥]

[†]Centre for Nanohealth, College of Engineering, University of Swansea, Singleton Park, SA2 8PP, United Kingdom

[‡]Institute for Materials Research, University of Leeds, Leeds, LS2 9JT, United Kingdom

[§]Cardiff Catalysis Institute, School of Chemistry, Cardiff University, Park Place, Cardiff, CF10 3AT, United Kingdom

[∥]Multidisciplinary Nanotechnology Centre, Department of Physics, College of Science, University of Swansea, Singleton Park, SA2 8PP, United Kingdom

[⊥]Multidisciplinary Nanotechnology Centre, College of Engineering, University of Swansea, Singleton Park, SA2 8PP, United Kingdom

S *Supporting Information*

ABSTRACT: Vertical arrays of nanostructures have been widely used as major components in some of the most ground-breaking modern research-based devices, and ZnO nanowires have received particular attention because of their favorable electronic properties. Using a local multiprobe technique to measure the properties of individual ZnO nanowires in vertical arrays, we show for the first time that for metal-catalyzed ZnO nanowire growth the electrical contribution of individual wires to a device is highly dependent on the fate of the catalyst nanoparticle during growth. To overcome the limitations of metal-catalyzed growth, nanowires grown from a defect-driven nucleation process are shown to provide high-quality device structures with excellent long-path electrical conduction.
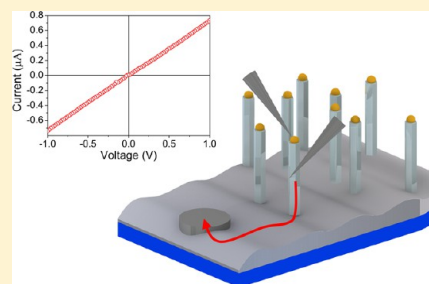
INTRODUCTION

ZnO nanowires are receiving a great deal of attention because of promising applications in electronic, optoelectronic, and electro-mechanical devices.[1−3] These devices typically rely on the electronic properties of the nanowires and utilize them in a range of configurations, from single-nanowire field-effect transistors (FETs)[4] and core−shell p-n structures,[5] to vertical array devices that use forests of aligned nanowires. A particular advantage of the array design is the fact that the single-crystal nanowires are in the final device configuration after a simple growth procedure. This is a bottom-up technology that allows the nanowire properties to be defined by the parameters set during manufacture rather than modified with complicated processing and low-yield fabrication techniques such as lithography. Hence, some of the most ground-breaking devices using ZnO nanowires are based upon as-grown arrays that stand perpendicular to a planar substrate.[1,6] In these devices, hundreds, thousands, or even millions of nanowires may function in parallel as they are electrically contacted at the base and at the tip; however, it has not been feasible in such a configuration of tightly packed structures to investigate the contribution an individual nanowire may provide to a complete device. Electrical measurement of an array device as a complete system samples a convolution of effects stemming from at least three structures: the nanowire top contacts, the nanowires, and the crystal growth that forms at the base which acts to interconnect adjacent columns (base growth layer). Optimizing

each of these components is an opportunity to enhance device performance but is technically demanding because of the difficulty in measuring such structures. Typical single-probe measurement techniques such as atomic force microscopy (AFM) and scanning tunneling microscopy (STM) are not able to distinguish between the conduction that occurs through the contact, nanowire, or base layer.[7−10] To overcome this and isolate measurements on the three components, we use a multiprobe ultrahigh vacuum (UHV) instrument that makes it possible to separate and distinguish between the electronic properties of each component. This capability removes ambiguous effects experienced with single-probe techniques that can include simultaneously measuring through multiple interfaces, sampling materials of varying dimensions, or relying on conduction through a substrate of dissimilar composition that can obscure the intrinsic information that is sought. The multiprobe technique has been successfully applied to measure the intrinsic electronic properties of individual ZnO nanowires in a flat-lying configuration[11] and when the nanowires are free-standing, which allows measurement of individual top contacts.[12] Korte et al. and Durand et al. have used similar experimental equipment orientating free-standing nanowires such that the side length of the structures was accessible to four

metal probes; this made it possible to measure the resistance profile along free-standing GaAs nanowires and the transport properties of metallic-like InAs nanowires, respectively.[13,14] Finally, to complete our understanding of ZnO nanowires in an array configuration, we applied the multiprobe technique to study the long-path electrical conduction from individual nanowires in as-grown arrays through the base growth to the large area Ohmic contact used for charge injection. We show here the quality of the long conduction path is equally important as the properties of the nanowires themselves; particularly, in any array device that is developed on an insulating substrate such as has been used for nanogenerators[15] and lasers,[6] transparent devices using various forms of glass,[16] and flexographic roll-to-roll printed devices.[17] For these devices the long conduction path can involve charge transport over large length scales (>500 μm) as the Ohmic contact must be formed to the side of the array where it forms an interface with the base layer. Therefore, the quality of the base growth is often paramount when optimizing the electronic output of a device. This requirement is confirmed by the multiprobe measurements that were conducted on arrays from two different nanowire growth methods.

When an array device is being designed, it is desirable to use a crystal growth method that provides control over the growth site, establishing the capability to pattern the nanowire forest. For this reason, a great deal of research has gone into the fundamental understanding of the vapor—liquid—solid (VLS) process that takes advantage of a metal catalyst to nucleate growth.[18−23] However, the VLS process is an extremely complex physical and chemical process with new evidence continually showing it is different for each nanowire material.[24] Irrespective of these permutations, the metal-catalyzed growth techniques provide a distinct advantage in controlling the nucleation site and subsequent nanowire position on the substrate. In this work, we examine with our measurement technique such nanowire arrays grown with the aid of a metal catalyst and show that the effectiveness of the electrical connection of the individual nanowires to the array can vary beyond expected fluctuations in nanowire properties. This has not been identified before by single-probe measurement techniques such as AFM and STM as they form one contact to the nanowire tip and measure the signal that passes through the entire array structure,[15] often registering a current of only nanoamps when conducted on ZnO.[8] We show much greater long-path current magnitudes (microamps) are possible with ZnO nanowires, and a current of nanoamps is effectively a nanowire that does not contribute to the device. To investigate the features that lead to small long-path currents, nanowire arrays were analyzed in cross section with transmission electron microscopy (TEM), showing large variations in the base crystal growth that interconnects the nanowire forest and revealing extensive contamination from the catalyst metal. Therefore, to overcome this problem, we explore a growth technique which maintains the patterning capability of metal-catalyzed growth by using a weak chemical etch of the surface to nucleate growth.[25] However, as no detailed understanding of the process or the final crystal quality has previously been reported, our understanding of the growth process is completed here. The improved method produces arrays of superior electronic properties that make ideal structures for vertical array devices.

■ MATERIALS AND METHODS

Nanowire Growth. ZnO nanowires were grown using carbothermal reduction of a powder ZnO source within a tube furnace.[1] Single-crystal ($11\bar{2}0$) α-Al$_2$O$_3$ was used to provide an excellent lattice match for growing hexagonal ZnO nanowires. For Au-catalyst-assisted growth, Au was deposited in thicknesses of 2−6 nm by plasma sputtering onto the solvent-cleaned substrate. The growth parameters used were as follows: furnace temperature, 900 °C; substrate temperature, 900 °C; pressure, 30 mbar; gas flow, 49 sccm Ar and 1 sccm O$_2$; and growth time, 30−120 min.

Single-crystal α-Al$_2$O$_3$ substrates for defect-driven growth were cleaned with solvents and rinsed before etching in 1 M NaOH for 5 min.[25] After being etched, the substrates were rinsed thoroughly with DI water, ethanol, and an additional water rinse and dried. Etching was performed with stirring at room temperature. Nanowire growth was then performed in a tube furnace with the following experimental parameters: furnace temperature, 1050 °C; substrate temperature, 600−650 °C; pressure, 1.6 mbar; gas flow, 100 sccm Ar and 10 sccm O$_2$; growth time, 60 min.

Electron Microscopy Analysis. Scanning electron microscopy (SEM) was used to examine the products from each growth experiment, particularly the morphology, alignment, and areal density. The SEM instrument used in this study was the Hitachi S4800 cold field emission gun SEM apparatus equipped with YAG BSE backscatter detector with resolution of 3 nm.

Transmission electron microscopy (TEM) analysis was carried out using a FEI Tecnai TF20 FEGTEM (200 keV) fitted with a Gatan Orius SC600 CCD camera. Nanowire array/substrate cross sections were prepared by focused ion beam (FIB) using a FEI Nova 200 NanoLab dual beam SEM/FIB instrument fitted with a Kleindiek micromanipulator for in situ lift-out. Sections of several microns length and a thickness of approximately 100 nm were prepared from arrays produced by both growth techniques. TEM energy dispersive X-ray spectroscopy (EDX) analysis was performed using an Oxford Instruments 80 mm^2 X-Max SDD fitted to the microscope and running INCA software.

Roughness Measurements. A JPK Nanowizard II atomic force microscopy (AFM) instrument was used in intermittent contact mode with RTESP and NCHV Bruker probes to image the surface of the substrates, and the processed data was used for roughness measurements. These results were validated with white light interferometry measurements using a Nikon BS-w 501 profilometer.

Electrical Measurement Technique. The Omicron LT Nanoprobe located at Swansea University, U.K. and the Omicron UHV Nanoprobe located at Leeds University, U.K. and also at Omicron GMBH, Germany were used to perform the electrical measurements. Each instrument comprises four individual W probes guided by a high-resolution Gemini FEG-SEM. This equipment configuration makes it is possible to form reversible, nondestructive electrical contacts to an individual as-grown nanostructure without any processing. The electrical measurements were conducted with a Keithley 2601 or Keithley 2636B source meter. The probes were electrochemically etched in 2 M KOH with 15 V DC supply applied through the 0.25 mm W wire.

The nanowire arrays were loaded into the load lock of the nanoprobe and pumped down until the vacuum pressure of

10^{-9} mbar was reached. The substrate was then transferred to the main chamber with the transfer arm. The probes were current-annealed within the chamber to remove oxides and contaminants in a manner that maintained the probe sharpness before mounting onto the measurement stage. All experiments were conducted at pressure of 10^{-10} mbar using the in situ SEM for imaging of the probes while they were manipulated close to the surface with full STM piezo control. It was then possible to directly contact a nanowire without the feedback loops by careful manual control of the coarse and fine piezo-motors, which have nanometer precision. SEM was essential for this process and allowed the operator to view the probes interacting with the nanowire. Current−voltage measurements of the individual nanowires were performed with two probes positioned on the nanowires, while long-path conduction measurements were performed between a probe on the nanowire side and the large area Ohmic contact, formed by silver paste or Ta strips used to fix the sample to the measurement plate. During long-path conduction measurements the sample was set at floating potential and the probe potential was swept ±1 V.

To assess the resistivity of the base layer films, four-probe measurements were conducted within the UHV system with four W probes placed equidistant apart in a straight line configuration with a separation of several hundred microns.

RESULTS AND DISCUSSION

Metal-Catalyzed Nanowire Measurements. Contacting individual nanowires in an array has previously proved problematic but is essential for allowing characterization of the structures in the as-grown state. This is desirable as the ZnO surface is highly sensitive to any processing or surface modification which can significantly change the measured properties. The ideal technique is to contact and measure individual nanowires with more than one probe simultaneously in contact with the free-standing nanostructure (see Methods and a previous report detailing four-probe measurements on nanowires for additional details[11]), as shown in Figure 1. In this configuration, with two probes on the nanowire, it was possible to establish low-resistance contacts directly on the structure of interest, which removed ambiguous effects that may result from unstable or rectifying contacts. The probe contacts in this
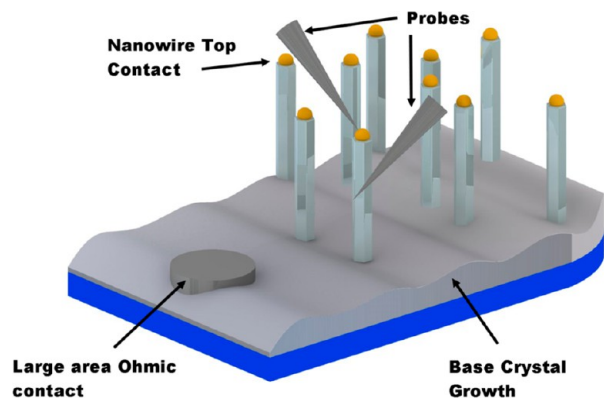

Figure 1. Schematic diagram showing a nanowire array complete with top contacts, base crystal growth, and large area Ohmic contact formed to the side of the array. The probes positioned on the nanowire show the configuration in which the multiprobe technique was used to take the I−V measurements.

configuration were tested and shown to be Ohmic before a measurement was taken. Typically, for ZnO nanowires, a current magnitude of hundreds of nanoamps up to several microamps was measured between the two probes. However, most importantly for array devices, the final probe configuration (Figure 1) made it possible to measure the long-path conduction between the side probe contact and the large area Ohmic contact formed to the perimeter of the nanowire array.

Applying this method to a ZnO nanowire array grown on single-crystal $(11\bar{2}0)$ α-Al_2O_3 (substrate) using Au catalyst in a high-temperature vapor phase process, we show that neighboring nanowires can have very different connections to the array (a series of measurements from each probe on a metal-catalyzed nanowire are shown in Figure S1 of the Supporting Information). Figure 2a (red) shows a current of ~700 nA at 1
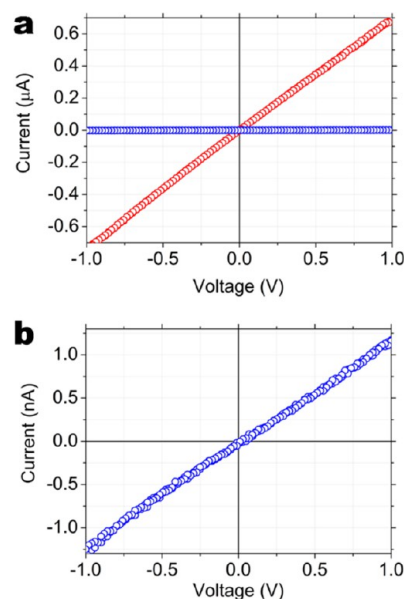

Figure 2. Current−voltage measurements taken with the multiprobe technique are plotted for two separate nanowires within a metal-catalyzed array. (a) The I−V measurement shows conduction from the probe on the side of one nanowire (red) to the large area Ohmic contact that is expected for typical ZnO nanowire electrical properties. However, another nanowire in the same array has a very poor electrical connection (blue), highlighted in (b), when measured in the same long-path probe configuration.

V was measured from the nanowire side probe contact through the base growth to the large area Ohmic contact; however, for another nanowire in the same array, little more than 1 nA at 1 V was measured (Figure 2a (blue) and in more detail in Figure 2b). When using a single-probe technique this information may be discarded and the measurement assumed to be dominated by a bad contact formed by the probe or, alternatively, the nanowire is considered to be a poor conductor. However, when we examine the nanowire from Figure 2b in more detail, we find that originally a current of 10 μA was measured between the two probes when both were positioned on the nanowire; the nanowire was one of the most conductive nanowires measured in this investigation. Indeed, for the 10 nanowires that were measured in this way, 4 were shown to have good connection to the array with currents from the nanowire to the large area Ohmic contact >200 nA, while 4 nanowires had long-path current between 10 nA and 70 nA, and 2 nanowires had virtually no electrical connection at all with ~1 nA at 1 V bias.
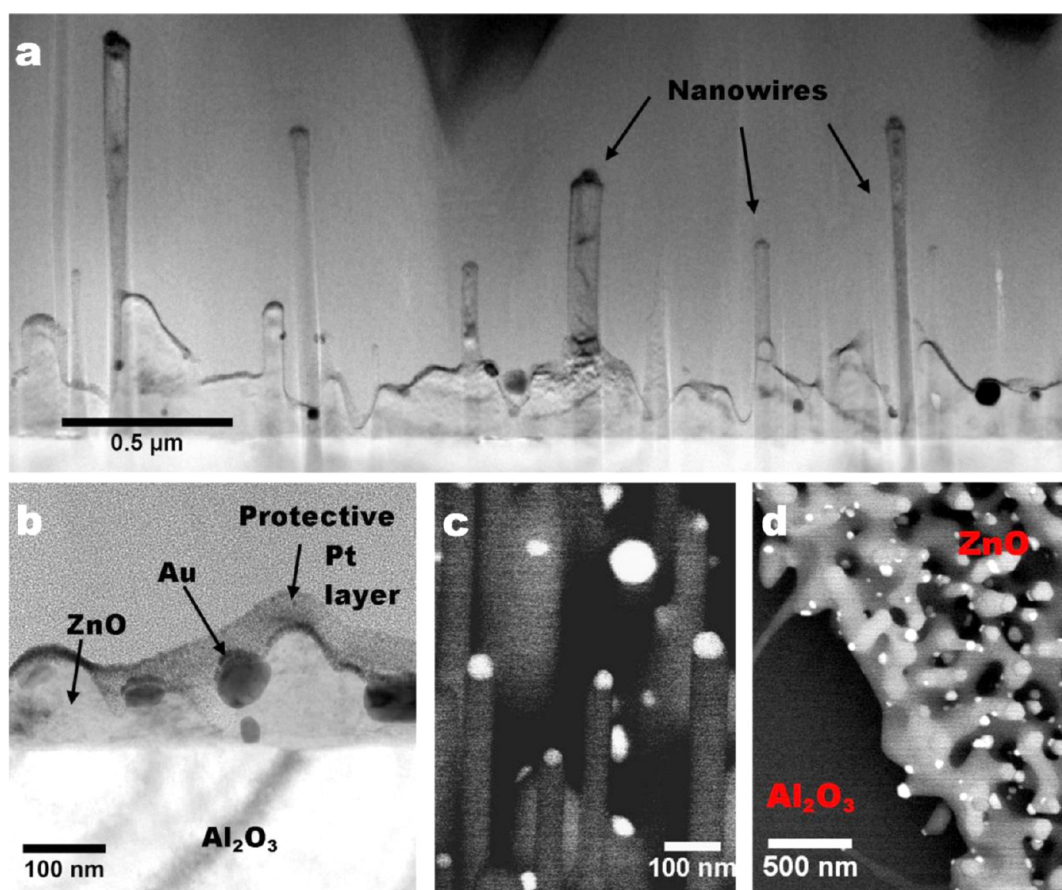
Figure 3. Electron microscopy images investigating metal-catalyzed ZnO nanowire growth. (a) A bright field TEM image of a cross section from a metal-catalyzed nanowire array showing the variability of the base growth and the random dispersion of Au particles (black) across the crystal film; panel (b) highlights these features in more detail. (c) BSE imaging was used to identify the catalyst particles (bright) on the nanowire tips; however, in panel (d), the top-down BSE image shows Au particles are found scattered across the growth.

(The complete electrical measurement data set is shown in Figure S2 of the Supporting Information.)

Examination of the Growth Structure. Therefore, it is important for the progress of nanowire array devices to establish the source of the large variability in electrical connection (depicted by Figure 2) that an individual nanowire can have with the array. We have already established during the measurement process the nanowires themselves or the contacts formed by the probes cannot be the source of error. Importantly, the variability in conduction must lie with the properties of the base crystal growth that interconnects adjacent nanowires. To investigate this crystal growth in detail, cross-sectional samples were prepared with focused ion beam milling and examined with TEM.

Figure 3a shows a bright field TEM image of a typical FIB cross-section taken from a metal-catalyzed array that indicates the ZnO growth is formed of a base crystal layer from which nanowires emerge and strike vertically upward. Two features are immediately distinct: first, Au particles (dark in the image) are found not only on the nanowire tips but also on the base growth; second, the base growth is highly variable, ranging from several hundreds of nanometers thickness to less than 50 nm. Inspecting in more detail (Figure 3b), we can see the Au particles vary in morphology and size and are spread across the base growth, and in some instances particles are embedded within the ZnO (Figure S3 of the Supporting Information). Additionally, Figure 3b shows the Au particles are found where the base layer is thinnest, suggesting this is the most energetically favorable position during the high-temperature growth when the particles are mobile. The combination of these two features may lead to areas of the array, or individual nanowires, being electrically isolated, as the presence of the metal in the semiconductor ZnO will undoubtedly lead to depletion regions.[26] Examining an array with SEM backscatter electron imaging (BSE) (Figure 3c), to highlight heavy elements, showed the nanowires have Au catalyst particles on the nanowire tips. However, when viewed top-down (Figure 3d), Au particles are also found dispersed extensively across the surface of the entire ZnO base layer that grows between the substrate and nanowire base. Depletion regions in the thinnest sections of the base layer lead to regions of electrical pinch-off which force current flow to take a longer more convoluted path through the sprawling base growth. For a nanowire sprouting out of the base on an electrically isolated region, this effect consequently reduces the current to nanoamperes. Scattering and other losses are only exacerbated by the line defects (shown in Figure S3 of the Supporting Information along with further TEM analysis in Figure S4), such as dislocations, that are found randomly distributed throughout the entire base ZnO matrix; these defects are not a feature of the nanowires, which have always been found to be single-crystal and defect-free.[11] To confirm these conclusions from the TEM analysis, the electrical measurements were correlated to the morphology and composition of the surrounding ZnO base layer for the metal-
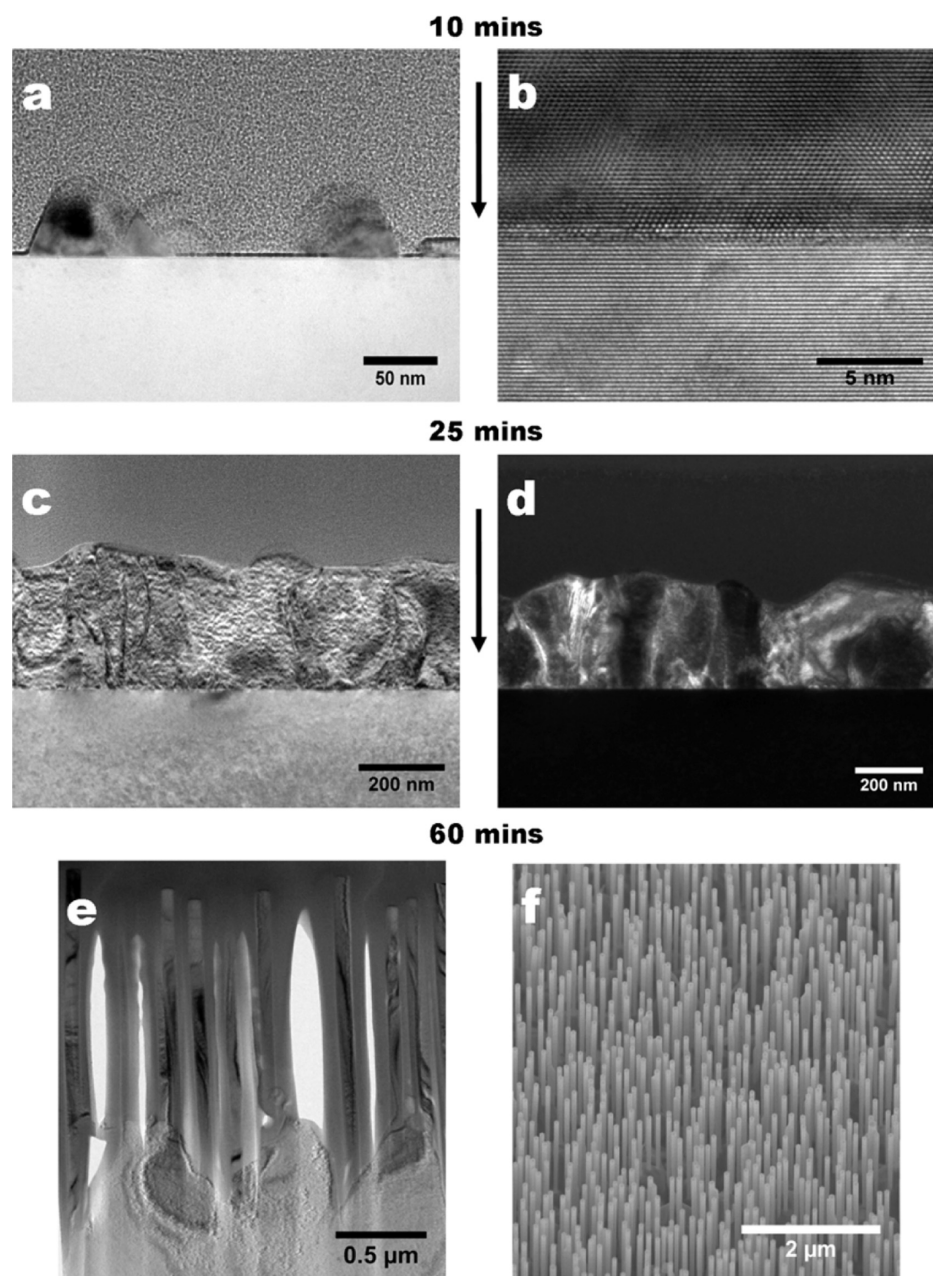
Figure 4. Electron microscopy images of cross-sectional samples as the etch-assisted growth progressed. (a) A bright field TEM image showing the initial stages of growth began with nucleation of nanoislands in lattice alignment with the substrate, as shown by a lattice image of the interface (b). After 25 min, the temperature increased and more source vapor encouraged further growth. The islands coalesced into a polycrystalline film in panel (c), and the grains are highlighted by a dark field image in panel d. After the full growth time, a dense array of perfectly aligned nanowires with a robust single-crystal base layer was produced, shown in bright field TEM image (e) and SEM image (f).

catalyzed nanowires using SEM and BSE (shown Figure S5 in the Supporting Information).

Optimizing with Etch-Assisted Growth. The highlighted deficiencies that include the variable base growth and contamination from the metal catalyst are a common feature among nanowire materials grown using this technique; hence, a great deal of focus has been applied to controlling the growth site and base growth such that only Au is found on the nanowire tips.[27−29] However, this may require several processing steps, and full control is not always achieved as a nanowire does not always grow from a catalyst particle. Figure 3d highlights the desirable patterning capability of metal-catalyzed growth and shows the abrupt control over growth site

that is possible when the Au is patterned on the substrate before growth is initiated; nanowires grow only where the catalyst is present. Therefore, a method that provides control over growth site and produces a high-quality large area base layer while simultaneously removing the requirement for a metal catalyst would be the ideal solution. A seldom-used technique which offers such promise is that of etch-assisted nanowire growth, which exposes the substrate surface to a reactive wet chemical etch. Consequently, vapor−solid growth is nucleated on the treated surface in a one-step growth process to form the base conducting layer and nanowire array.[25] Only a small number of investigations by the group of Lin at National Tsing Hua University, Taiwan have used this technique, and no

thorough investigation into the growth method has been reported, despite its effectiveness in producing patterned growth for devices.[30] Here we analyze this method in detail to test the suitability for array devices and show growth is nucleated by an increase in surface defects.

When the growth progression was examined, it was apparent growth was initiated on the single-crystal $(11\bar{2}0)$ α-Al$_2$O$_3$ (substrate) after a short period (10 min) when the substrate reached ~500 °C and crystalline nanoislands nucleated that were oriented with the $[0001]$ direction perpendicular to the substrate (Figure 4a,b). As growth proceeded (25 min) and the temperature increased to ~550 °C, the islands merged forming a polycrystalline layer (Figure 4c,d) that created a continuous film. This beneficial feature ensured that all nanowires that subsequently grew in the array were physically connected by the same ZnO crystal layer. With continuing growth to 600 °C (45−60 min), nanowires emerged and the base layer grew thicker (Figure 4e), forming a substantial robust film that appeared to be one single crystal across the entire growth area, and one which could be tailored to cover several tens of square millimeters (Figure 4f). On completion of the full growth time, the boundaries between grains found in the intermediate film growth disappeared with very few defects found in the bulk of the array; the high-quality and vertically aligned growth of the nanowire array is a result of the favorable lattice mismatch (~0.08%) of ZnO on a-plane sapphire.[3,31,32] This is in contrast to observations made in GaN films grown on Al$_2$O$_3$, where high densities of threading dislocations can occur because of lattice mismatch between the film and the substrate.[33] Importantly, no boundaries were observed at the junction between the nanowire and base layer which together form one continuous crystal (shown Figure S6 in the Supporting Information). However, some line defects were observed around the base of the nanowires at the physical connection with the base layer. To test whether these defects may influence the electrical output, we measured the nanowires in the as-grown array in a way similar to that used for the metal-catalyzed nanowires. All nanowires exhibited excellent conduction in the long-path configuration (Figure 5), and of 19 nanowires a current of at
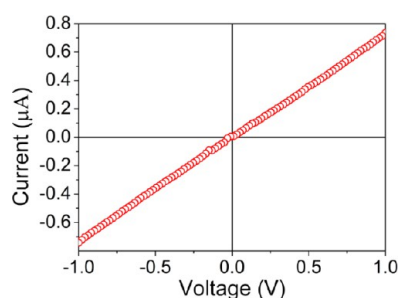

Figure 5. Current−voltage measurements of the long current path using the multiprobe technique of a nanowire within an etch-assisted growth array.

least ~150 nA at 1 V bias was measured from the nanowire side to the large area Ohmic contact. Significantly, the majority of nanowires measured current between 400 nA to 1 μA at 1 V; only 3 nanowires measured a current less than 250 nA (but greater than 150 nA) at 1 V, which can be explained by variations in nanowire conductivity.

Defect-Driven Growth Characterization. To fully characterize the crystal growth produced by this method,

four-probe measurements were conducted using the multiprobe instrument on the polycrystalline film growth shown in Figure 4c. Measurements showed the film to be highly conductive with a resistivity of 0.085 ± 0.0175 Ω cm, which is similar to that of single-crystal nanowires and typical of ZnO thin films grown in an oxygen-rich atmosphere.[34] The low resistivity of the ZnO film ensured the long-path voltage drop across the base layer was negligible as we measured a four-probe resistance of only 630 Ω at a probe separation of ~280 μm (in comparison, the metal-catalyzed base layer resistance was measured to be 1900 Ω over a similar length scale). When compared to that of a connecting nanowire, typically having a resistance of >100 kΩ, the high quality of the base layer maintains the measured long-path current with minimal losses when compared to metal-catalyzed growth. Importantly, the base layer has such a low resistance that it overcomes the need for an additional conductive layer or conductive substrate that is often assumed to be necessary for efficient electronic devices using nanowire arrays. This device-compatible property will preserve the signal produced by all nanowires in the array and confirms the effectiveness of the etch-assisted growth technique for ZnO nanowires in vertical array devices.

Ho et al.[25] have suggested that the etching process leads to an increased surface roughness which in turn provides preferential growth nucleation sites. However, using AFM and optical profilometry no difference in roughness could be measured between as-received wafers, substrates that were annealed at 900 °C, and substrates that were etched; with AFM, an RMS roughness of ~60−100 pm was measured, showing the samples were all similar to epi-polished wafers (see Figure S7 and Table 1 of the Supporting Information). This is consistent with the relatively mild etching of Al$_2$O$_3$ to be expected from dilute NaOH.[25]

From TEM images (Figure 6) it is apparent that the nanoislands of ZnO often form at defective regions of the substrate surface including step edges (Figure 6a) and line defects such as dislocations (Figure 6b) that were located within a few subsurface crystal planes. A previous report by Morin and Jin showed ZnO nanowires can nucleate at screw dislocations on etched GaN where etching was used to remove surface oxides and organics revealing the underlying defects in the crystalline substrate.[35] As Al$_2$O$_3$ has no additional surface oxide phase, the surface contamination that remains after solvent cleaning will be mainly due to organics, the majority of which will be removed by the etching process which also reacts with the Al$_2$O$_3$ lattice. Therefore, from the TEM analysis it is thought the surface chemical reaction of the etching process induces various forms of defects that act as accommodation sites.[36] Etching at defective areas on the surface of the Al$_2$O$_3$ substrate is likely to be more effective than etching at areas with higher order which may lead to the heavy twinning that was observed within the nanoislands where a high concentration of surface defects was found (Figure 6c). It is worth recalling at this point that defects in the ZnO base layer identified in the early stages of growth near the Al$_2$O$_3$ interface were not observed in the later stages of growth, which is most likely due to the temperature being higher once nanowire growth is initiated and the defects being annealed out. However, the presence of lattice defects such as those observed with TEM may not be the only favorable sites for nucleation.
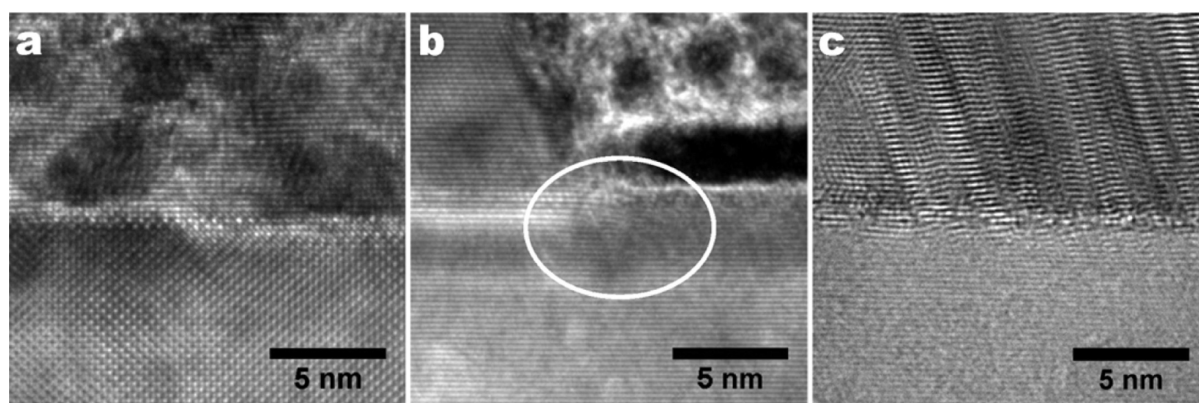
$$Al_2O_3 + 2NaOH + 3H_2O \rightarrow 2Na^+ + 2Al(OH)_4^- \qquad (1)$$
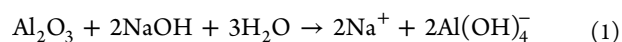
Figure 6. Lattice images of surface defects that are typically found at island growth sites in the early stages of growth. (a) Step edge where a growth island had nucleated. (b) Dislocations can extend to the subsurface planes of the substrate, and (c) twinning in the ZnO island was observed when a high density of surface defects was present.

The absence of an observable increase in roughness also suggests the etching process has an impact at much smaller length scales; we can speculate that the etching extracts aluminum ions from the lattice (eq 1), leading to high-energy adsorption sites where the ZnO can nucleate.[36] An oriented crystalline ZnO growth develops from the nucleation points growing into a continuous film over the substrate, but we can expect the original sites of nucleation to be somewhat thicker than the rest of the film, and it is likely that these sites serve as points for nanowire growth to proceed. Once the conditions favor nanowire growth this is maintained until on completion, a continuous forest of dense but evenly spaced nanowires covers the entire etched region of the substrate.

Growth on untreated Al_2O_3 exhibited only a very low density of nanowires that did not have an interconnecting base layer and had seemingly grown from native defects in the as-received wafer. A defect-driven growth process is a simple technique that can be applied to other material systems with the correct choice of chemical reactants. Most importantly, the growth method produces a high quality conductive layer that interconnects all nanowires in the array without inhibiting the device output.

We have shown the electrical conduction of ZnO nanowires in an array device configuration can be maximized by utilizing a defect-driven growth process. This was confirmed using a multiprobe method that allows the individual components of an array to be measured in isolation without any modification to the growth structure. When the need for a metal catalyst to nucleate growth was removed, the base crystal growth was high-quality and free from any metal catalyst contamination. This ability to control the composition and growth site coupled with the excellent electrical properties make the growth structure ideal for vertical array devices that rely on the parallel output of individual nanowires.

ASSOCIATED CONTENT

ⓢ Supporting Information

Additional electrical measurments, TEM/EDX data, and AFM data. This material is available free of charge via the Internet at http://pubs.acs.org.

AUTHOR INFORMATION

Corresponding Author

*E-mail: a.m.lord@swansea.ac.uk.

Author Contributions

#These authors contributed equally

Notes

The authors declare no competing financial interest.

REFERENCES

(1) Lu, M.-P.; Lu, M.-Y.; Song, J.; Chen, M.-T.; Gao, Y.; Chen, L.-J.; Wang, Z. L. Piezoelectric Nanogenerator Using P-Type ZnO Nanowire Arrays. *Nano Lett.* **2009**, *9*, 1223−1227.

(2) Gao, P. X.; Song, J.; Liu, J.; Wang, Z. L. Nanowire Piezoelectric Nanogenerators on Plastic Substrates as Flexible Power Sources for Nanodevices. *Adv. Mater. (Weinheim, Ger.)* **2007**, *19*, 67−72.

(3) Yang, P.; Yan, H.; Mao, S.; Russo, R.; Johnson, J.; Saykally, R.; Morris, N.; Pham, J.; He, R.; Choi, H.-J. Controlled Growth of ZnO Nanowires and Their Optical Properties. *Adv. Funct. Mater.* **2002**, *12*, 323−331.

(4) Hong, W.; Sohn, J. I.; Hwang, D.; Kwon, S.-S.; Jo, G.; Song, S.; Kim, S.; Ko, H.-J.; Park, S.-J.; Welland, M. E.; et al. Tunable Electronic Transport Characteristics of Surface-Architecture-Controlled ZnO Nanowire Field Effect Transistors. *Nano Lett.* **2008**, *8*, 950−956.

(5) Fickenscher, M.; Shi, T.; Jackson, H. E.; Smith, L. M.; Yarrison-Rice, J. M.; Zheng, C.; Miller, P.; Etheridge, J.; Wong, B. M.; Gao, Q.; et al. Optical, Structural, and Numerical Investigations of GaAs/AlGaAs Core−Multishell Nanowire Quantum Well Tubes. *Nano Lett.* **2013**, *13*, 1016−1022.

(6) Chu, S.; Wang, G.; Zhou, W.; Lin, Y.; Chernyak, L.; Zhao, J.; Kong, J.; Li, L.; Ren, J.; Liu, J. Electrically Pumped Waveguide Lasing from ZnO Nanowires. *Nat. Nanotechnol.* **2011**, *6*, 506−510.

(7) Timm, R.; Persson, O.; Engberg, D. L. J.; Fian, A.; Webb, J. L.; Wallentin, J.; Jönsson, A.; Borgström, M. T.; Samuelson, L.; Mikkelsen, A. Current−Voltage Characterization of Individual As-Grown Nanowires Using a Scanning Tunneling Microscope. *Nano Lett.* **2013**, *13*, 5182−5189.

(8) Park, W. I.; Yi, G.-C.; Kim, J.-W.; Park, S.-M. Schottky Nanocontacts on ZnO Nanorod Arrays. *Appl. Phys. Lett.* **2003**, *82*, 4358−4360.

(9) Léonard, F.; Talin, A.; Swartzentruber, B.; Picraux, S. Diameter-Dependent Electronic Transport Properties of Au-Catalyst/Ge-Nanowire Schottky Diodes. *Phys. Rev. Lett.* **2009**, *102*, 106805.

(10) Salehzadeh, O.; Chen, M. X.; Kavanagh, K. L.; Watkins, S. P. Rectifying Characteristics of Te-Doped GaAs Nanowires. *Appl. Phys. Lett.* **2011**, *99*, 182102.

21183

dx.doi.org/10.1021/jp505414u | *J. Phys. Chem. C* 2014, 118, 21177−21184

(11) Lord, A. M.; Maffeis, T. G.; Walton, A. S.; Kepaptsoglou, D. M.; Ramasse, Q. M.; Ward, M. B.; Köble, J.; Wilks, S. P. Factors That Determine and Limit the Resistivity of High-Quality Individual ZnO Nanowires. *Nanotechnology* **2013**, *24*, 435706.

(12) Lord, A. M.; Walton, A. S.; Maffeis, T. G.; Ward, M. B.; Davies, P.; Wilks, S. P. ZnO Nanowires with Au Contacts Characterised in the as-Grown Real Device Configuration Using a Local Multi-Probe Method. *Nanotechnology*, accepted for publication, **2014**

(13) Korte, S.; Steidl, M.; Prost, W.; Cherepanov, V.; Voigtländer, B.; Zhao, W.; Kleinschmidt, P.; Hannappel, T. Resistance and Dopant Profiling along Freestanding GaAs Nanowires. *Appl. Phys. Lett.* **2013**, *103*, 143104.

(14) Durand, C.; Berthe, M.; Makoudi, Y.; Nys, J.-P.; Leturcq, R.; Caroff, P.; Grandidier, B. Persistent Enhancement of the Carrier Density in Electron Irradiated InAs Nanowires. *Nanotechnology* **2013**, *24*, 275706.

(15) Wang, Z. L.; Song, J. Piezoelectric Nanogenerators Based on Zinc Oxide Nanowire Arrays. *Science* **2006**, *312*, 242−246.

(16) Park, H.; Chang, S.; Jean, J.; Cheng, J. J.; Araujo, P. T.; Wang, M.; Bawendi, M. G.; Dresselhaus, M. S.; Bulović, V.; Kong, J.; et al. Graphene Cathode-Based ZnO Nanowire Hybrid Solar Cells. *Nano Lett.* **2013**, *13*, 233−239.

(17) Lloyd, J. S.; Fung, C. M.; Deganello, D.; Wang, R. J.; Maffeis, T. G. G.; Lau, S. P.; Teng, K. S. Flexographic Printing-Assisted Fabrication of ZnO Nanowire Devices. *Nanotechnology* **2013**, *24*, 195602.

(18) Allen, J. E.; Hemesath, E. R.; Perea, D. E.; Lensch-Falk, J. L.; LiZ, Y.; Yin, F.; Gass, M. H.; Wang, P.; Bleloch, A. L.; Palmer, R. E.; et al. High-Resolution Detection of Au Catalyst Atoms in Si Nanowires. *Nat. Nanotechnol.* **2008**, *3*, 168−173.

(19) Bar-Sadan, M.; Barthel, J.; Shtrikman, H.; Houben, L. Direct Imaging of Single Au Atoms within GaAs Nanowires. *Nano Lett.* **2012**, *12*, 2352−2356.

(20) Kirkham, M.; Wang, X.; Wang, Z. L.; Snyder, R. L. Solid Au Nanoparticles as a Catalyst for Growing Aligned ZnO Nanowires: A New Understanding of the Vapour−Liquid−Solid Process. *Nanotechnology* **2007**, *18*, 365304.

(21) Brewster, M. M.; Zhou, X.; Lim, S. K.; Gradečak, S. Role of Au in the Growth and Nanoscale Optical Properties of ZnO Nanowires. *J. Phys. Chem. Lett.* **2011**, *2*, 586−591.

(22) Adhikari, H.; Marshall, A. F.; Chidsey, C. E. D.; McIntyre, P. C. Germanium Nanowire Epitaxy: Shape and Orientation Control. *Nano Lett.* **2006**, *6*, 318−323.

(23) Wang, G. T.; Talin, A. A.; Werder, D. J.; Creighton, J. R.; Lai, E.; Anderson, R. J.; Arslan, I. Highly Aligned, Template-Free Growth and Characterization of Vertical GaN Nanowires on Sapphire by Metal−Organic Chemical Vapour Deposition. *Nanotechnology* **2006**, *17*, 5773−5780.

(24) Ross, F. M. Controlling Nanowire Structures through Real Time Growth Studies. *Rep. Prog. Phys.* **2010**, *73*, 114501.

(25) Ho, S.-T.; Chen, K.-C.; Chen, H.-A.; Lin, H.-Y.; Cheng, C.-Y.; Lin, H.-N. Catalyst-Free Surface-Roughness-Assisted Growth of Large-Scale Vertically Aligned Zinc Oxide Nanowires by Thermal Evaporation. *Chem. Mater.* **2007**, *19*, 4083−4086.

(26) Rhoderick, E. H.; Williams, R. H. *Metal-Semiconductor Contacts*; Clarendon Press: Oxford, U.K., 1988.

(27) Kim, D. S.; Scholz, R.; Gösele, U.; Zacharias, M. Gold at the Root or at the Tip of ZnO Nanowires: A Model. *Small* **2008**, *4*, 1615−1619.

(28) Subannajui, K.; Güder, F.; Zacharias, M. Bringing Order to the World of Nanowire Devices by Phase Shift Lithography. *Nano Lett.* **2011**, *11*, 3513−3518.

(29) Fan, H. J.; Zacharias, M. Manipulation of Crawling Growth for the Formation of Sub-Millimeter Long ZnO Nanowalls. *J. Mater. Sci. Technol. (Shenyang, China)* **2009**, *24*, 589−593.

(30) Ho, S.-T.; Wang, C.-Y.; Liu, H.-L.; Lin, H.-N. Catalyst-Free Selective-Area Growth of Vertically Aligned Zinc Oxide Nanowires. *Chem. Phys. Lett.* **2008**, *463*, 141−144.

(31) Baxter, J. B.; Aydil, E. S. Epitaxial Growth of ZnO Nanowires on a- and c-Plane Sapphire. *J. Cryst. Growth* **2005**, *274*, 407−411.

(32) Fons, P.; Iwata, K.; Yamada, A.; Matsubara, K.; Niki, S.; Nakahara, K.; Tanabe, T.; Takasu, H. Uniaxial Locked Epitaxy of ZnO on the a Face of Sapphire. *Appl. Phys. Lett.* **2000**, *77*, 1801.

(33) Ning, X. J.; Chien, F. R.; Pirouz, P.; Yang, J. W.; Khan, M. A. Growth Defects in GaN Films on Sapphire: The Probable Origin of Threading Dislocations. *J. Mater. Res.* **1996**, *11*, 580−592.

(34) Craciun, V.; Elders, J.; Gardeniers, J. G. E.; Boyd, I. W. Characteristics of High Quality ZnO Thin Films Deposited by Pulsed Laser Deposition. *Appl. Phys. Lett.* **1994**, *65*, 2963.

(35) Morin, S. A.; Jin, S. Screw Dislocation-Driven Epitaxial Solution Growth of ZnO Nanowires Seeded by Dislocations in GaN Substrates. *Nano Lett.* **2010**, *10*, 3459−3463.

(36) Saunders, R. B.; McGlynn, E.; Henry, M. O. Theoretical Analysis of Nucleation and Growth of ZnO Nanostructures in Vapor Phase Transport Growth. *Cryst. Growth Des.* **2011**, *11*, 4581−4587.